To: George F GAO[gaof@im.ac.cn]
Cc: Shi, Pei yong[peshi@UTMB.EDU]; Tseng, Chien-Te K.[sktseng@UTMB.EDU]
From: LeDuc, James W.[/O=EXCHANGELABS/OU=EXCHANGE ADMINISTRATIVE GROUP (FYDIBOHF23SPDLT)/CN=RECIPIENTS/CN=937DF08E29C4439E88A04BABFFB162AD-JWLEDUC]
Sent: Thur 1/16/2020 1:55:36 PM (UTC-06:00)
Subject: new Coronavirus
Chinese Response to New Virus Shows Promise_Le Duc-14Jan20.docx
Lethal and nonlethal ACE2 transgenic mouse lineages_2009.pdf

Hi George,

Congratulations on China's response to the emergence of another new coronavirus. Under your strong leadership, you and your colleagues have prepared China well for this new threat and I think that it is important that your efforts are recognized. The link below is to an article published earlier this week in WIRED magazine where I am quoted on the stark differences in response between SARS and now. In addition, I just submitted the attached essay to the Houston Chronicle as an Op Ed. I haven't heard yet if it has been accepted, but if they don't take it, I'll try elsewhere. This is a good story at a time when we need one.

As you might expect, we are following the evolving story on nCoV from Wuhan very closely and we are eager to get an isolate for antiviral testing. Dr Tseng's lab here in the GNL has developed a transgenic mouse model for SARS that is very useful and we are anxious to see if it can be used for the nCoV as well. Any suggestions on how we might obtain an isolate would be most appreciated, and if you would like to send an investigator here to the GNL to work with Dr Tseng on the antiviral screening and further development of the animal model, we would welcome the collaborations. A copy of his publication is attached.

With best wishes,

Jim

Here's a link to the story, which published this morning.

James W. Le Duc, Ph.D.
Director
Galveston National Laboratory
University of Texas Medical Branch
Galveston, TX 77555-0610
(t) 409-266-6500
(f) 409-266-6810
(m) 409-789-2012

Chinese Response to New Virus Shows Promise

Fast action and open communications by China may be saving the world from another devastating infectious disease outbreak. Many will recall the dark days in the spring of 2003 when Asia and the world were threatened by the appearance of a new virus disease, Severe Acute Respiratory Syndrome, or SARS, which first appeared in southern China and quickly spread to other countries around the world, ultimately causing over 8000 cases with nearly 10% of those ending in death. SARS was caused by a novel coronavirus then unknown to medical science. There was no known cure, no diagnostic tests and little understanding of where it came from or how it was spread, although person-to-person transmission was obvious as health care workers treating the first cases were themselves among the early victims. Initially, China was reluctant to share information or alert the international community of the magnitude of the epidemic, leading to international criticism and a dangerous global health situation. Fortunately, under pressure, China reversed its position, opened its borders to collaborations with the WHO, U.S. and others, and the epidemic was eventually controlled.

Today, another novel coronavirus has been discovered, again in China; however, this time, less than two decades later, things are very different. Chinese health officials recognized that a new disease had emerged, quickly isolated the patients, and instituted an impressive set of interventions to limit the spread of disease and characterize the new pathogen. Importantly, they have been very transparent in sharing their findings with the world, thus allowing other nations to be on the lookout for the new disease. The outbreak is still in the early stages and fortunately, preliminary results suggest that the new virus is not easily transmitted from person-to-person. While only about 40 patients have been identified, there has been at least one death, and a patient is now hospitalized in Thailand, having traveled from the outbreak site in Wuhan, China. The genome of the new virus was completely sequenced and posted for easy access by experts around the world, allowing rapid exploration of possible treatments, development of diagnostics and epidemiological investigations.

China's ability to respond quickly and efficiently to this new threat is the result of nearly two decades of investments and collaborations to improve public health in China. The Chinese Centers for Disease Control incorporates many of the strengths of our own CDC, but is designed to meet the needs of a 1.4 billion plus population. In addition, China has invested in building a robust scientific capacity and partnered with containment laboratories such as ours to incorporate best practices when studying dangerous pathogens.

The current outbreak clearly demonstrates a new openness to health information sharing with the global community. To diagnose an outbreak early requires astute healthcare providers able to recognize when something new or unusual is occurring; however, clinical recognition alone is meaningless if there is no capacity to investigate the cases or characterize the disease-causing agent.

For the last few years, the D.C.-based National Academy of Science, Engineering and Medicine has worked with the Chinese Academy of Sciences to build relationships and share information on emerging diseases and advancements in the development of vaccines and treatments. In Galveston, we have welcomed leading Chinese health officials to learn about biocontainment facility design and construction, biosafety training and laboratory operations. These collaborations, along with U.S.-based educational opportunities for Chinese students, benefit us all.

China's response to the new coronavirus clearly demonstrates that their investments both in physical laboratories and scientific diplomacy over the past decade are paying dividends, not only to China, but the entire world. Since infectious diseases do not recognize international borders, much must still be done with this current and quickly evolving situation, including the sharing of clinical material, information on containment and treatment options. The international community can assist with studies to determine the original source of infection, assumed to be zoonotic.

At a time when US-China relations are being tested, it is important to note that relations within the public health and scientific research arenas remain positive, which is a success story worth sharing.

James Le Duc, PhD, is the Director of the Galveston National Laboratory at the University of Texas Medical Branch and a professor in UTMB's Department of Microbiology and Immunology.

684 words

JOURNAL OF VIROLOGY, June 2009, p. 5451–5465 Vol. 83, No. 11
0022-538X/09/$08.00+0 doi:10.1128/JVI.02272-08

Differential Virological and Immunological Outcome of Severe Acute Respiratory Syndrome Coronavirus Infection in Susceptible and Resistant Transgenic Mice Expressing Human Angiotensin-Converting Enzyme 2[▽]

Naoko Yoshikawa,[1] Tomoki Yoshikawa,[1] Terence Hill,[1] Cheng Huang,[1] Douglas M. Watts,[2] Shinji Makino,[1] Gregg Milligan,[3] Tehsheng Chan,[1] Clarence J. Peters,[1,2,4] and Chien-Te K. Tseng[1,4]*

Departments of Microbiology and Immunology,[1] Pathology,[2] and Pediatrics[3] and Center for Biodefense and Emerging Infectious Disease,[4] University of Texas Medical Branch, Galveston, Texas 77555-0609

Received 29 October 2008/Accepted 10 March 2009

We previously reported that transgenic (Tg) mice expressing human angiotensin-converting enzyme 2 (hACE2), the receptor for severe acute respiratory syndrome coronavirus (SARS-CoV), were highly susceptible to SARS-CoV infection, which resulted in the development of disease of various severity and even death in some lineages. In this study, we further characterized and compared the pathogeneses of SARS-CoV infection in two of the most stable Tg lineages, AC70 and AC22, representing those susceptible and resistant to the lethal SARS-CoV infection, respectively. The kinetics of virus replication and the inflammatory responses within the lungs and brains, as well as the clinical and pathological outcomes, were assessed in each lineage. In addition, we generated information on lymphocyte subsets and mitogen-mediated proliferation of splenocytes. We found that while both lineages were permissive to SARS-CoV infection, causing elevated secretion of many inflammatory mediators within the lungs and brains, viral infection appeared to be more intense in AC70 than in AC22 mice, especially in the brain. Moreover, such infection was accompanied by a more profound immune suppression in the former, as evidenced by the extensive loss of T cells, compromised responses to concanavalin A stimulation, and absence of inflammatory infiltrates within the brain. We also found that $CD8^+$ T cells were partially effective in attenuating the pathogenesis of SARS-CoV infection in lethality-resistant AC22 mice. Collectively, our data revealed a more intense viral infection and immunosuppression in AC70 mice than in AC22 mice, thereby providing us with an immunopathogenic basis for the fatal outcome of SARS-CoV infection in the AC70 mice.

Severe acute respiratory syndrome coronavirus (SARS-CoV) emerged as a public health threat in November 2002, and by July 2003 this previously unknown virus had spread to 29 countries in five continents. This outbreak resulted in more than 8,000 cases and 774 deaths and was accompanied by a devastating social, economic, and medical impact worldwide (15). It is generally believed that the reservoirs of SARS-CoV are the Chinese horseshoe bat (*Rhinolophus sinicus*), palm civet cat, and other exotic animal species. These species are sold in markets as sources of food for human consumption and are believed to be responsible for the first cases in southern China (16, 20). Currently, it is a matter of debate as to whether SARS-CoV will make the transition from animals to humans or if such a transition will again result in a global pandemic. However, SARS-CoV and the conditions that fostered the first outbreak continue to exist in southern China, posing a threat for its reemergence. Thus, effective prophylactic or therapeutic strategies against SARS beyond supportive care are needed should reemergence of the virus occur in the future.

The exact mechanism of SARS pathogenesis remains unknown. Evidence has shown that SARS-CoV is transmitted by large droplets, likely via aerosol or fecal-oral routes, with the lungs being the main pathological target. SARS patients exhibited a wide-ranging clinical course, characterized mainly by fever, dry cough, dyspnea, lymphopenia, various degrees of pancytopenia, arterial hypoxemia, and rapidly progressing changes in chest radiography (15). Studies with postmortem lung tissues revealed diffuse alveolar damages, with prominent hyperplasia of pneumocytes, and an increased accumulation of activated macrophages. Strikingly, these pulmonary manifestations usually occurred after the clearance of viremia and in the absence of infections by other opportunistic agents. The pulmonary damage in SARS patients could be caused directly by viral destruction of permissive alveolar and bronchial epithelial cells. Such a delay in revealing reactive hemophagocytosis and other pathological manifestations within the lungs of patients severely affected by SARS strongly suggested that overly intense host inflammatory responses to the infection may play a major role in the pathogenesis of SARS. The likelihood of SARS being an immune-mediated disease was further supported by the highly elevated expression of various innate inflammatory cytokines in the circulation of SARS patients, a state commonly referred to as a "cytokine storm" (1, 3, 24, 30). However, in the absence of recurring SARS epidemics, an

* Corresponding author. Mailing address: Department of Microbiology and Immunology, University of Texas Medical Branch, 301 University Boulevard, G.150 Keiller Building, Galveston, TX 77555-0609. Phone: (409) 747-0789. Fax: (409) 747-0762. E-mail: sktseng@utmb.edu.

▽ Published ahead of print on 18 March 2009.

animal model that mimics human disease is critical for defining the exact cellular and molecular basis of SARS pathogenesis, in order to develop effective preventive and therapeutic strategies against SARS.

The animal species permissive for SARS-CoV infection include mice (young and aged) and some of their derivatives, e.g., "knockout" and transgenic (Tg) mice, hamsters, ferrets, and various nonhuman primates. Unfortunately, infection in these animal models does not result in clinical diseases resembling those reported for human SARS cases (26, 29), and in the case of primates, the costs of studying them are quite high. We have focused our studies on characterizing the pathogenesis of SARS-CoV infection in Tg mice expressing human angiotensin-converting enzyme 2 (hACE2), the functional receptor of SARS-CoV (19), established in our laboratories. Our initial characterization from two different lineages of hACE2 Tg mice (AC70 and AC63) clearly demonstrated that the Tg expression of hACE2 makes the otherwise resistant mice highly susceptible to SARS-CoV infection, resulting in an overwhelming infection, especially in the lungs and brains of both lineages, accompanied by a clinical illness of varying severity (32). Specifically, mice of the AC70 lineage developed an acute wasting syndrome that resulted in 100% mortality within a week following the infection, whereas AC63 mice eventually recovered from the diseases without suffering any mortality, despite progressive weight loss and other signs of illness. Although SARS likely stems from an unregulated and often excessive inflammatory response, the exact nature of the host responses and their correlation with the severity of the diseases associated with SARS-CoV infection are not entirely clear. The exhibition of such a strikingly different final outcome to SARS-CoV infection, i.e., lethal versus nonlethal, among lineages of hACE2 Tg mice makes it useful for establishing the correlates between host responses and SARS pathogenesis. The small litter size and the inconsistent hACE2 expression in AC63 mice led us choose the other lethality-resistant hACE2 Tg lineage, AC22, for the subsequent characterization of host responses to SARS-CoV infection.

In this study, we infected hACE2 Tg AC70 and AC22 mice with an equal amount of SARS-CoV (i.e., 10^6 50% tissue culture infective doses [$TCID_{50}$]) to compare the correlates between various aspects of host immune responses (e.g., proinflammatory cytokines, modulation of lymphocyte subsets, and mitogen-induced proliferation of lymphocytes) and the pathogenesis of SARS-CoV infection. The data presented in this study extend our previously reported observations concerning the differential pathogenesis of SARS-CoV infection in hACE2 Tg mouse lineages that are either highly susceptible or resistant to lethality following SARS-CoV infection. We believe that our results provide insight into the cellular and molecular basis of host immune responses relevant to the final outcome of murine SARS-CoV infection.

MATERIALS AND METHODS

Mice. Tg mice expressing human ACE2 were generated as previously described (32). Among the five established Tg lineages, three (i.e., AC12, AC50, and AC70) and two (i.e., AC22 and AC63) were susceptible and resistant to lethality in response to SARS-CoV, respectively (Table 1). The tissue expression profiles of hACE2 in AC22 and AC70 mice were developed following semiquantitative reverse transcription-PCR (RT-PCR) by using hACE2-specific primers (forward, 5′-AGGATGTGCGAGTGGCTA-3′; reverse, 5′-AGGGCCATCAG GATGTCC-3′), as we previously described (35). For this study, we chose the AC70 and AC22 lineages, which are two of the most stable lines with regard to hACE2 expression, breeding efficiency, and litter size.

TABLE 1. Differential outcome of hACE2 Tg mouse lineage to SARS-CoV infection

Transgenic lineage	$TCID_{50}$ (log_{10}) of SARS-CoV (Urbani strain)	Morbidity (weight loss, etc.)	Mortality (%)	Mean survival time (days p.i.)
AC70	3	+	100	6.2
AC50	3	+	100	6.9
AC12	3	+	100	4.5
AC22	6	+	0	—[a]
AC63	6	+	0	—

[a] —, not applicable.

In some experiments, $CD8^+$ T-cell-depleted Tg AC22 mice were used for assessing the role of this T-cell subset in the host responses against SARS-CoV infection. To deplete $CD8^+$ T cells, we injected (intraperitoneally [i.p.]) two doses (50 μg/per dose, 3 days apart) of anti-mouse CD8 monoclonal antibody (clone 2.43) or an isotype-matched rat immunoglobulin G (IgG) antibody (clone SFR8) as controls. The extent of depletion was assessed at day 2 after the last antibody treatment by obtaining splenocytes and analyzing them for the presence of $CD3^+$ $CD8^+$ T cells by flow cytometry. To ensure a persistent state of cell depletion during the course of SARS-CoV infection, we treated Tg AC22 mice with either anti-CD8 antibody or control antibody at days −4, −1, +2, +5, and +8, where day 0 was defined as the time of SARS-CoV challenge.

SARS-CoV and cells. The Urbani strain of SARS-CoV, kindly provided to us by T. G. Ksiazek, Centers for Disease Control and Prevention (Atlanta, GA), was used throughout this study. Vero E6 cells (ATCC) were used for virus infectivity assays. The original stock of SARS-CoV, designated passage 1, received two additional passages in Vero E6 cells. The titer of this last passage 3 was determined and expressed as $TCID_{50}$/ml, and the virus was stored at −80°C, and used throughout this study. All experiments involving infectious virus were conducted at the University of Texas Medical Branch, Galveston, TX, under an animal use and care protocol approved by the University of Texas Medical Branch IACUC in AALAC-accredited animal biosafety level 3 and biosafety level 3 laboratories.

Infection of mice, body weight, illness score, and mortality. Anesthetized Tg mice, their non-Tg littermates, and $CD8^+$ T-cell-depleted Tg mice, ranging from 8 to 20 weeks of age, were infected intranasally (i.n.) with 60 μl of SARS-CoV in phosphate-buffered saline (PBS) that contained the indicated doses of infectious virus. Control mice were inoculated with the same volume of PBS. Infected mice were weighed daily to allow us to monitor disease progression. In addition, the severity of illness in infected mice was scored independently by two investigators who used a previously described (9), standardized 1-to-5 grading system as follows: 0, healthy; 1, barely ruffled fur; 2, ruffled fur but active; 3, ruffled fur and inactive; 4, ruffled fur, inactive, and hunched; and 5, dead. In some experiments, infected mice were sacrificed at indicated time intervals to obtain lungs and brains for determining viral infectivity titers, staining for viral antigen by immunohistochemistry (IHC), profiling the inflammatory responses, and analyzing the histopathology. We also harvested the spleens of uninfected and SARS-CoV-infected Tg mice at days 2 and 4 in separate experiments to determine CD4 T-cell, CD8 T-cell, B-cell, and non-T- non-B-cell subsets and their response to concanavalin A (ConA) stimulation as described below.

Virus titers in the lungs and brains of infected mice. The lungs and brain specimens obtained from mice at the indicated time points after infection were weighed and homogenized in a PBS–10% fetal calf serum solution using the TissueLyser-Qiagen (Retsch, Haan, Germany) to yield 10% tissue suspensions. After clarification by centrifugation, serial 10-fold dilutions of the tissue suspensions were prepared and assayed in Vero E6 cells to determine viral titers (32). The titers of individual samples were expressed as $TCID_{50}$ per gram of tissues.

IHC and histopathology. Lung and brain tissues, obtained as described above, were fixed in 10% neutral buffered formalin, embedded in paraffin, and processed for the subsequent IHC and histopathology studies, as described previously (32). Briefly, 5-μm sections were used to detect the expression of SARS-CoV nucleocapsid (N) protein by using standard IHC by sequential incubation with rabbit-specific anti-SARS-CoV N protein antibody, phosphatase-conjugated secondary antibodies, and naphthol-fast red (as a substrate). Slides were coun-

terstained with hematoxylin, and antigen expression was examined under different magnifications. The hematoxylin-eosin-stained paraffin sections were used for routine histopathological studies.

Cytokine and chemokine profiling. Gamma-irradiated lung and brain homogenates were subjected to inflammatory profiling by using the 23-plex Cytometric Bead Array (Bio-Rad, Hercules, CA), as described previously (32).

Flow cytometry and ConA-induced proliferation of splenocytes. Splenocytes were stained for fluorescein isothiocyanate- or phycoerythrin-conjugated anti-CD3, -CD4, -CD8, -B220, and -CD14 and their corresponding isotype-matched control antibodies (all from CalTag Laboratories). These samples were then analyzed with FACScan and CelQuest software (BD Biosciences), as described previously (33). For determining the capacity of splenocytes to proliferate in response to mitogen stimulation, we cultured 2×10^5 cells/200 μl in triplicate in 96-well, U-bottomed microtiter plates in the presence or absence of ConA (2.5 μg/ml; Sigma-Aldrich) for 3 days. The cultures were pulsed with 1 μCi/well [^{3}H]thymidine (New England Nuclear) for the last 12 to 16 h in the culture. The total incorporation of [^{3}H]thymidine was determined by liquid scintillation counting and expressed as counts per minute (cpm) or stimulation index, which was calculated as total cpm of ConA-stimulated cells/total cpm of unstimulated cells.

Statistical analysis. Statistical analyses were performed by using a two-tailed, unpaired Student *t* test. Unless otherwise indicated, means ± standard errors of the means are shown.

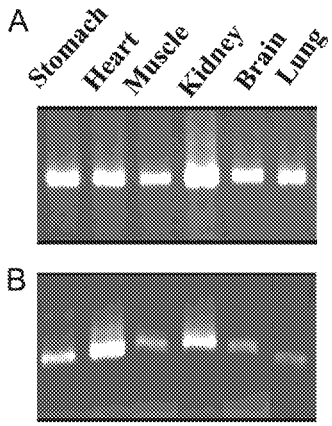

FIG. 1. Tissue expression profile of hACE2 in the Tg mouse lineages AC70 (A) and AC22 (B). DNA-free RNAs extracted from different organs of Tg mice at 6 to 8 weeks of age were subjected to RT-PCR analysis to evaluate the expression of hACE2 mRNA. The RT-PCR products were analyzed on 2% agarose gels. The data shown are representative of two independently conducted experiments.

RESULTS

Differential susceptibility of hACE2 Tg mice of different lineages to SARS-CoV infection. Our observations on the pathogenesis of SARS-CoV infection in two different lineages of hACE2 Tg mice, i.e., the AC70 and AC63 lineages, were reported previously (32). We continued to characterize the remaining three lineages with regard to their susceptibility, clinical manifestations (i.e., ruffled fur, lethargy, rapid and shallow breathing, and weight loss), and mortality, if any. As summarized in Table 1, all Tg lineages established were highly susceptible to infection compared to their non-Tg littermates. Like that of AC70 mice, infection of AC50 and AC12 mice with 10^3 $TCID_{50}$ of SARS-CoV resulted in the mice developing an acute wasting syndrome and eventually succumbing to the infection with a 100% mortality rate, with a mean survival time of less than 1 week postinfection (p.i.). While the 50% lethal dose of SARS-CoV for AC70 mice was approximately 1.7 log units, the prospective 50% lethal doses for AC50 and AC12 mice were not determined, largely due to the scarcity of the available animals. In contrast to the lethality-susceptible lineages, AC22 mice, following infection with up to 10^6 $TCID_{50}$ of SARS-CoV, survived despite exhibiting weight loss and other signs of clinical illness. Importantly, the transcriptional levels of hACE2 expression in various tissues of AC22 mice, especially those of the lungs and brain, were lower than those in Tg AC70 mice (Fig. 1). This observation was consistent with our earlier observation that Tg mice for which SARS-CoV infection was lethal (e.g., AC70 mice) had much higher levels of hACE2 expression than Tg mice for which infection was not lethal (e.g., AC63 mice) (32).

Differential SARS-CoV-induced morbidity and mortality between AC70 and AC22 mice. To further establish the possible correlates between host responses and such a strikingly different outcome of the infection, groups of 21 and 31 age-matched AC70 and AC22 mice, respectively, were inoculated (i.n.) with the same dose of SARS-CoV, i.e., 10^6 $TCID_{50}$/60 μl of SARS-CoV. Infected mice were monitored daily for morbidity and cumulative mortality, if any. In addition, three mice of each lineage were sacrificed at daily intervals until day 5 and three AC22 mice were also sacrificed at days 6, 8, 10, and 12, thereby allowing us to assess the infectivity titers of SARS-CoV in the lungs and brains, two of the most prominent tissues shown to support viral replication in our hACE2 Tg mice (32). As shown in Fig. 2, infected AC70 mice started to manifest various signs of illness, including ruffled fur, lethargy, rapid and shallow breathing, trembling, and immobility, accompanied by a relentless weight loss, starting at day 3 p.i. The weight loss of infected AC70 mice at day 3 was approximately 15%, and it reached up to 20% of the animals' total body weight before death by day 6 p.i. Despite their susceptibility to the infection, as evidenced by the progressive weight loss, which could reach an average of about 30%, infected AC22 mice gradually regained the lost weight, starting at day 9 p.i. In addition, infected AC22 mice exhibited a much milder disease than the infected AC70 mice and eventually recovered without suffering any mortality, which suggested to us that this lineage was indeed resistant to lethal infection by SARS-CoV.

Kinetics of viral replication in the lungs and brain. Based on the striking differences in the clinical symptoms as well as the mortality after SARS-CoV infection in AC70 and AC22 mice, we compared the kinetics and distribution of SARS-CoV replication in the lungs and brains between these two lineages. Viral replication in the lungs reached a maximum at day 1 p.i., in which averages of $10^{8.5}$ and $10^{8.7}$ $TCID_{50}$ SARS-CoV/gram were recovered from AC70 and AC22 mice, respectively, and gradually declined thereafter (Fig. 3). However, at day 5 p.i. a significantly higher level of viral replication was sustained in the lungs of a single surviving AC70 mouse than in any AC22 mice. A low-grade viral replication in the lungs of some infected AC22 mice continued until day 8 p.i. In contrast to the subtle dissimilarity of the viral replication in the lungs, the magnitudes and kinetics of viral infection within the brains of these two lineages were remarkably different. Specifically, a low level of infectious virus ($\sim 10^{2.7}$) was first detected in the brains of infected AC70 mice at day 2. Viral replication within this tissue proceeded rapidly thereafter, reached a maximum of $\sim 10^8$ $TCID_{50}$/g at day 3, and remained prominent through day

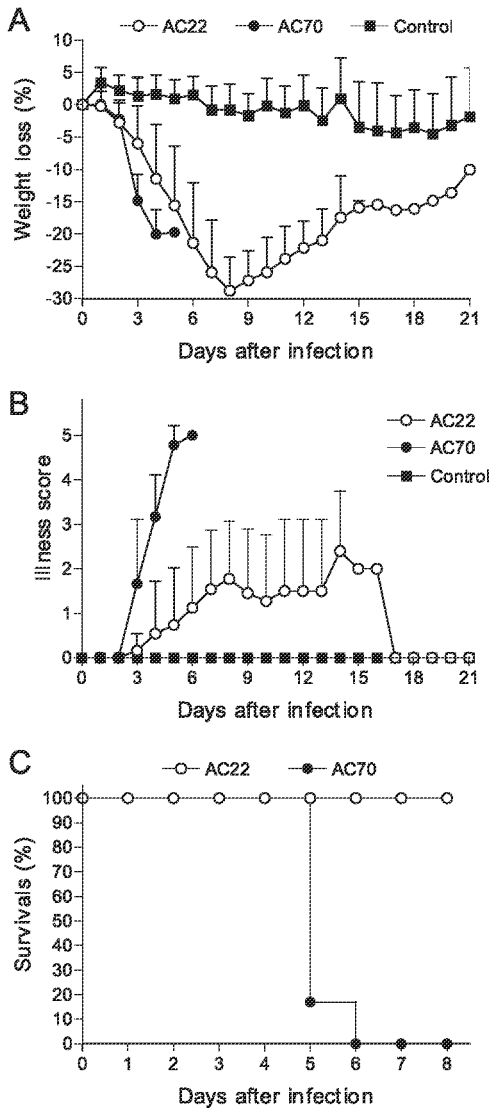

FIG. 2. Differential outcomes of SARS-CoV infection in AC70 and AC22 Tg mice. Groups of hACE2 Tg and age-matched non-Tg mice (control) (n = 14 to 31 mice/group) were infected intranasally with 10^6 $TCID_{50}$ of SARS-CoV (Urbani strain). The severity of clinical illness, i.e., weight loss (A), average illness score (B), and cumulative mortality (C), of infected mice was recorded daily as described in Materials and Methods. Error bars indicate standard deviations.

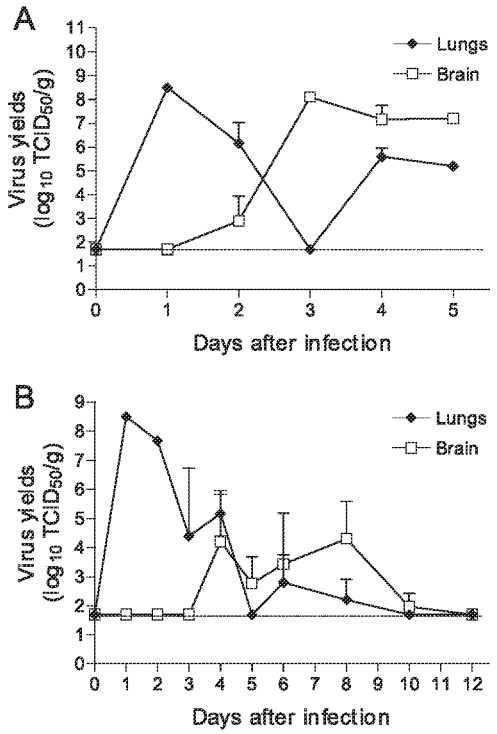

FIG. 3. Kinetics of viral replication in the lungs and brains of SARS-CoV-infected AC70 and AC22 mice. AC70 (A) and AC22 (B) mice were infected with SARS-CoV as described for Fig. 1. Three mice from each group were sacrificed at the indicated days after infection for determining infectious virus titers in the lungs and brains by the standard infectivity assay in Vero E6 cells. The viral titers were expressed as $\log_{10}$ $TCID_{50}$ virus per gram of tissue. Data are shown as means ± standard deviations for three animals at each time point, except for AC70 mice at day 5, where only one mouse survived the infection.

5, at which time a titer of ~10^7 $TCID_{50}$/g was routinely recovered. In contrast, SARS-CoV replication in the brains of infected AC22 mice was relatively benign, in that a modest level of infectious virus (~10^4) was initially demonstrated on day 4 and gradually declined to a barely detectable level at both days 8 and 10 p.i.

IHC and histopathology. The differential kinetics of viral replication and the final outcomes of SARS-CoV infection exhibited by AC70 and AC22 mice prompted us to investigate the temporal and spatial patterns of viral distribution and the pathological changes within the lungs and brains of infected animals. IHC staining for the SARS-CoV N protein clearly indicated that bronchiolar and alveolar epithelial cells and the neuronal cells were the primary targets of SARS-CoV infection in both Tg lineages. As shown in Fig. 4, an intense expression of viral antigen was first detected in the cytoplasm of bronchial epithelial cells, and occasionally in alveolar epithelial cells, at day 1. This viral antigen subsequently spread to the alveolar epithelial cells at day 2 but was undetectable within the lungs at day 3 and day 4 p.i. for the AC70 and AC22 mice, respectively. In contrast to its early expression within the lungs, SARS-CoV N protein in the brain was not detected until day 3 and day 4 in infected AC70 and AC22 mice, respectively (Fig. 5). Sustained expression of viral antigen was demonstrated until days 5 and 10 in the brains of AC70 and AC22 mice, respectively. This temporal expression of viral protein in the brain, as detected by IHC, was largely consistent with that revealed by the viral infectivity titers (Fig. 3).

Histopathological studies of the lungs did not reveal any obvious difference in the pulmonary pathologies between these two lineages, even though the infection-associated pathological process was faster in the AC70 than in the AC22 mice. Pathological changes in the lungs of both lineages started on day 1 and were characterized by a minimal-to-mild perivascular and peribronchiolar inflammatory infiltration, accompanied by the swelling and blebbing of epithelial cells lining bronchi and bronchioles (Fig. 6). Such a pathological process was followed by the accumulation of cell debris, necrotic epithelial cells, and

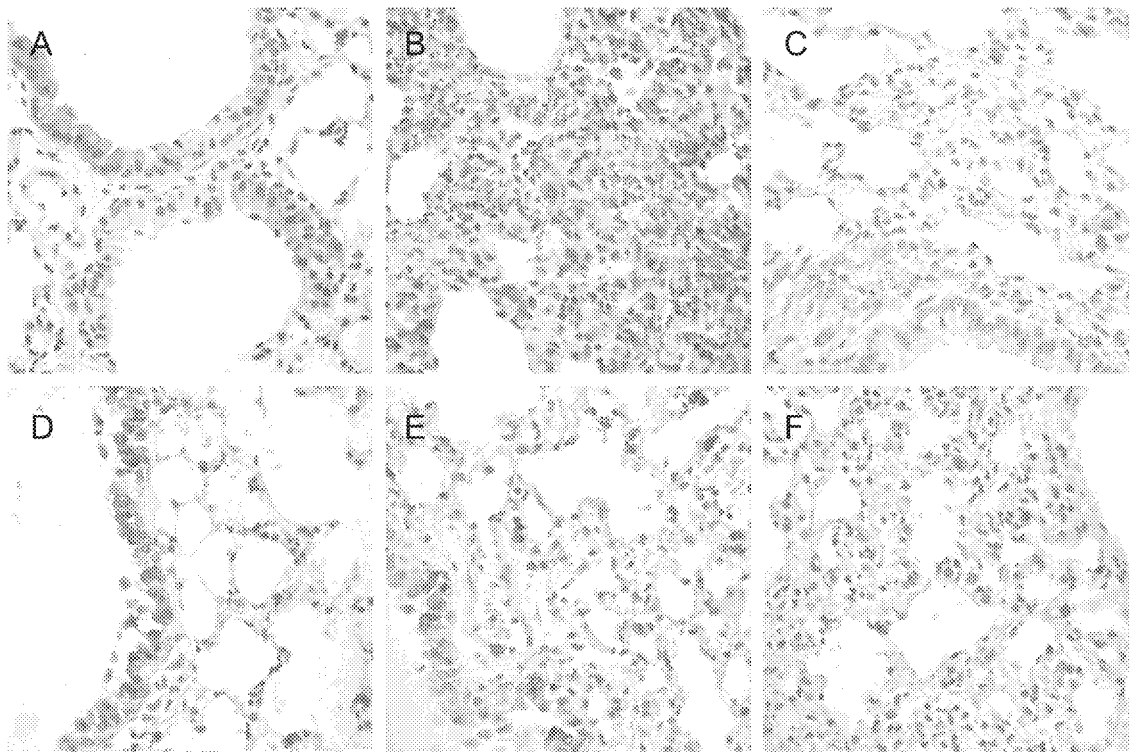

FIG. 4. SARS-CoV antigen expression in the lungs of AC70 and AC22 mice. Paraffin-embedded lung sections of SARS-CoV-infected AC70 mice (A to C) and AC22 mice (D to F) were analyzed for the expression of SARS-CoV nucleocapsid protein by IHC, as described in Materials and Methods. Profound viral infection, as indicated by the intense staining of viral antigen (red), was first detected in the cytoplasm of bronchial epithelial cells (A and D) at day 1, subsequently spread to the alveolar epithelial cells at day 2 (B and E), and subsided to either an undetectable level (C) or a lower level (F) in AC70 and AC22 mice at day 3, respectively. Original magnifications, ×40.

inflammatory cells within the bronchiolar lumen, along with interstitial thickening on day 2 p.i. As a consequence of reduced cellular infiltration, the interstitial thickening gradually subsided on day 3 in infected AC70 mice. In contrast, interstitial thickening intensified in infected AC22 mice until day 4 p.i. and was accompanied by infiltrating macrophages, pyknotic cells, and necrotic cells within the alveolar spaces. Mild inflammatory responses remained detectable in some areas of the lungs until day 4 and day 6 p.i for AC70 and AC22 mice, respectively.

Compared to the relatively indistinguishable pulmonary pathologies, a substantial difference in the pathologies of the brain was apparent between these two Tg lineages. Specifically, perivascular cuffing in the meninge and brain in the absence of other signs of inflammation was demonstrated infrequently in some AC70 mice at day 3 or day 4 p.i. (Fig. 7). In contrast, prominent perivascular lymphocytic cuffing in the meninge was consistently observed in AC22 mice on day 4 and spread to the brain parenchyma by day 5, where it was accompanied by a time-dependent infiltration of mononuclear cells within the central nervous system (CNS) until day 21 p.i., at which point the experiment was terminated. These results suggested that AC22 mice were superior to AC70 mice in mounting a full spectrum of inflammatory responses upon challenge by SARS-CoV.

Cytokine profiling of SARS-CoV-infected AC70 versus AC22 mice. SARS pathogenesis likely stems from exuberant acute inflammatory responses within the lungs (23). Our results that revealed the differential clinical and pathological outcomes between AC70 and AC22 mice in response to SARS-CoV infection led us to profile SARS-CoV-induced cytokine responses in these two Tg lineages by using BioPlex analysis. The results showed that AC70 mice were capable of secreting elevated levels of interleukin-12 p40 (IL-12p40), KC, RANTES, and monocyte chemoattractant protein 1 (MCP-1) in the lungs at at least one time point during the course of a 5-day infection, However, AC22 mice appeared to be more immunologically competent in mounting inflammatory responses, resulting in the production not only of the aforementioned cytokines at higher levels but also of three additional cytokines (IL-1α, IL-1β, and IL-6) that were not detected in infected AC70 mice (Fig. 8). Other cytokines, including IL-2, IL-3, IL-4, IL-5, IL-9, IL-10, IL-13, IL-17, gamma interferon, and tumor necrosis factor alpha, were not detected.

Cytokine responses were also measured in the brains of infected animals. The production of a total of 13 out of 23 cytokines that can be measured simultaneously, including IL-1α, IL-1β, IL-6, IL-8 (KC), IL-9, IL-10, IL-12p40, MIP-1α, MIP-1β, MCP-1, eotaxin, granulocyte colony-stimulating factor, and RANTES, was significantly induced in the brains of both Tg lineages at at least one time point during the entire course of infection (Fig. 9). Additionally, the kinetics and the magnitudes of the cytokine responses within each lineage appeared to positively correlate with the extent of virus replication (Fig. 3). However, there was no direct

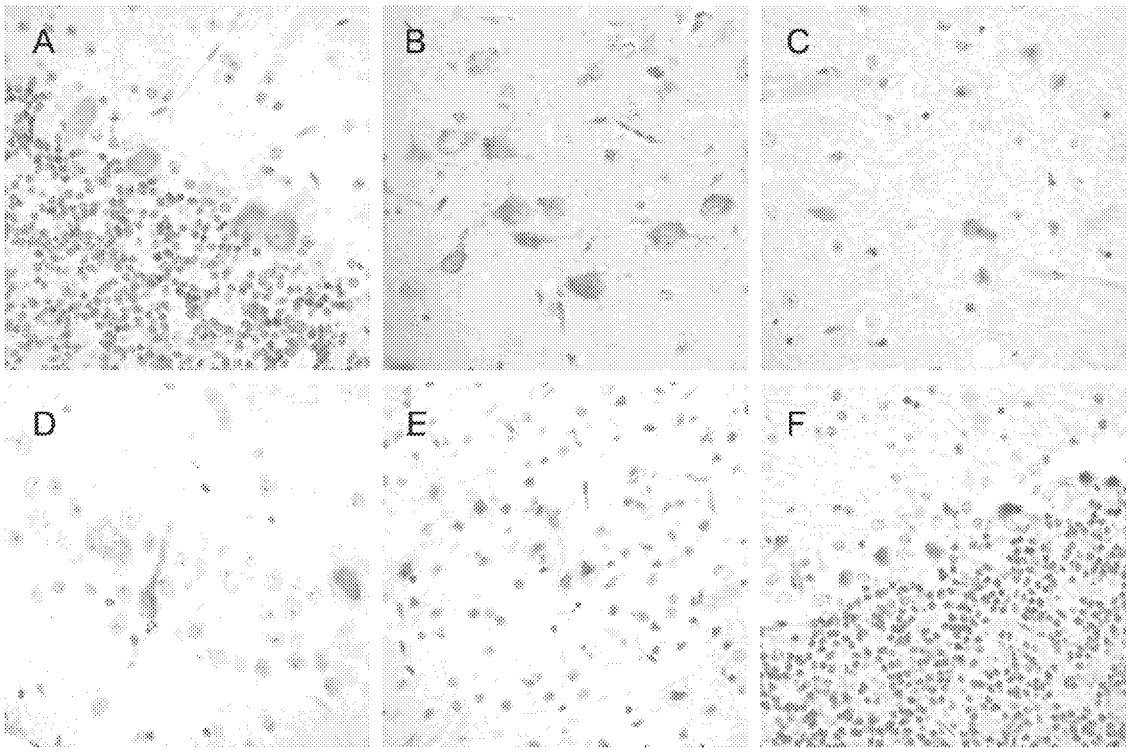

FIG. 5. SARS-CoV antigen expression in the brains of AC70 and AC22 mice. The brains of infected AC70 (A to C) and AC22 (D to F) mice were fixed, sectioned, and processed for the staining of SARS-CoV N protein as for Fig. 3. Viral antigen could be consistently detected in many neuronal cells of AC70 mice from day 3 (A) and remained readily detectable at days 4 and 5 (B and C). The earliest time for detecting viral antigen in the neuronal cells of infected AC22 mice was day 4 (D), and it remained detectable at days 6 and 10 after infection (E and F). Original magnifications, ×40.

correlation between the extent of viral replication and the magnitude of inflammatory responses when these two Tg lineages were compared. Specifically, despite much higher viral titers (~4 log units) detected in the brains of AC70 mice than in those of AC22 mice, such an overwhelming viral infection in AC70 mice failed to induce inflammatory cell infiltrates, a finding which was readily demonstrable in AC22 mice, in this organ (Fig. 7).

Alteration of the lymphocyte subsets and ConA-induced proliferation of splenocytes of infected mice. Many viruses are capable of immunoevasion to establish their infection. The compromised ability of infected AC70 mice to elicit a full-blown inflammatory response in the brain led us to question whether SARS-CoV could induce a generalized immunosuppression in the infected hosts. To evaluate the impact of SARS-CoV infection on the host immune response, both uninfected and infected AC22 and AC70 mice were sacrificed at days 2 and 4 p.i. for assessing the lymphocyte subsets and ConA-induced proliferation of splenocytes. While SARS-CoV infection did not result in any noticeable change in the total number of cells recovered and their constituents of the lymphocyte subsets at day 2 p.i. (data not shown), it caused a significant reduction in the total number of splenocytes, especially those of selected lymphocyte subsets, in these two lineages of Tg mice at day 4 p.i. compared to equivalent findings in uninfected mice (Table 2). Specifically, while SARS-CoV infection significantly reduced the number of recovered CD4 T cells ($P = 0.005$) in AC22 mice, it spared any profound impact on the total numbers of splenocytes, CD8 T cells, B cells, and non-T non-B cells. In contrast, SARS-CoV infection exerted a more profound impact in AC70 mice beyond significantly reducing the number of CD4 T cells in the spleen ($P = 0.025$). In fact, it also caused significant reductions in the total splenocytes ($P = 0.032$) and the CD8 T cells ($P = 0.001$). This marked reduction in the total numbers of T cells, especially the $CD8^+$ subset, in infected AC70 mice was further underlined by the significantly increased CD4/CD8 ratio ($P < 0.018$) compared to that in uninfected mice. Interestingly, similar to the case for AC22 mice, the populations of B cells and non-T non-B cells in the spleens of AC70 mice were not significantly altered upon challenge by SARS-CoV.

In addition to causing a striking reduction in the numbers of selected T-cell subsets, SARS-CoV infection significantly impaired ConA-mediated proliferation of splenocytes of both AC22 and AC70 mice ($P < 0.01$) compared to that in uninfected mice (Table 3; Fig. 10). Importantly, such a compromised ConA-mediated proliferative response observed in infected mice appeared to be more severe in AC70 than in AC22 mice ($P < 0.01$). Because ConA is a T-cell-specific mitogen, the more intense defect of infected AC70 than AC22 mice in responding to this mitogen was consistent with the more profound loss of splenic T cells in infected AC70 than in AC22 mice, i.e., 53% and 29%, respectively, compared to their uninfected controls.

Protective role of $CD8^+$ T cells against SARS-CoV infection in AC22 mice. While SARS-CoV infection drastically reduced

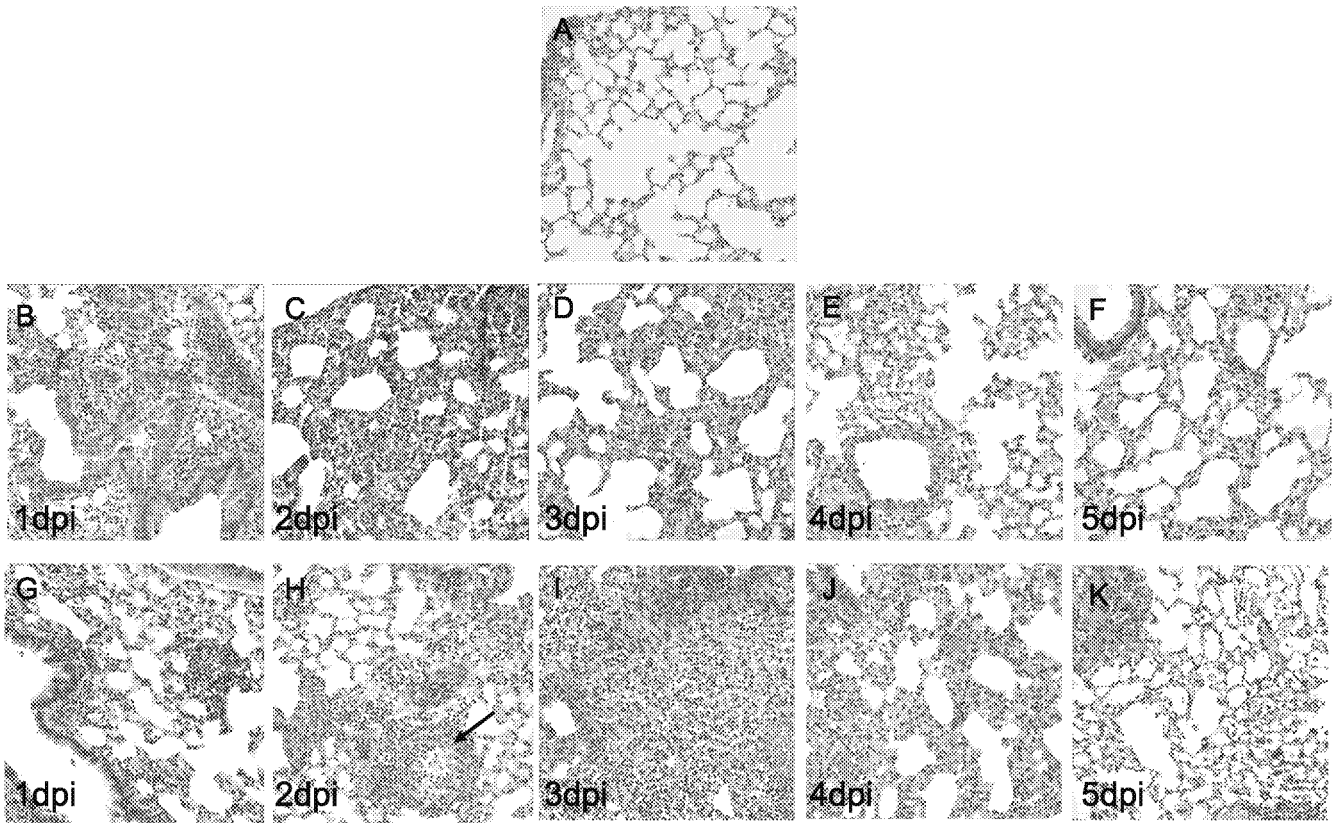

FIG. 6. Lung pathology of SARS-CoV-infected AC70 and AC22 mice. We examined paraffin-embedded, hematoxylin- and eosin-stained lung sections obtained from mock-infected (A) and SARS-CoV-infected AC70 (B to F) and AC22 (G to K) mice at the indicated time points after infection. Lung pathology in both lineages started at 1 day p.i. (dpi) (with mild mononuclear cell infiltration around blood vessels and bronchioles, accompanied by swelling and blebbing of epithelial cells of bronchi and bronchioles (B and G). Accumulation of cell debris within the lumen (arrow), interstitial thickening, and inflammatory cellular infiltrates were observed at day 2 (C and H). Peribronchial inflammation continued, as the damaged pneumocytes and disrupted epithelial lining were readily detectable through days 3 and 4 (B, I, E, and J) and gradually subsided thereafter, with a minimal-to-mild cellular infiltration observed at day 5 (F and K). Original magnifications, ×20.

the total numbers of $CD4^+$ and $CD8^+$ T-cell subsets in lethality-susceptible Tg AC70 mice, it significantly reduced only $CD4^+$, and not $CD8^+$, T cells in Tg AC22 mice (Table 2). To determine whether this largely intact $CD8^+$ T-cell subset might contribute to the relatively benign clinical and/or pathological phenotypes of infected AC22 mice, we infected CD8-depleted AC22 mice with SARS-CoV and monitored weight loss and the titers of infectious virus and pathology in the lungs and brain. As shown in Fig. 11A, treating Tg AC22 mice with only two doses of anti-mouse CD8 antibody, as described in Materials and Methods, was sufficient to deplete the great majority of CD8 T cells, compared to the numbers of these cells in control antibody-treated mice. Interestingly, depletion of CD8 T cells appeared to exacerbate pulmonary infection, as evidenced by the ~2-log-unit increase in the yields of infectious SARS-CoV within the lungs, but not the brain, at both days 2 and 4 p.i. (Fig. 11B), accompanied by the more prominent weight loss (Fig. 11C) and profound lung pathology (Fig. 11D) than those elicited in control antibody-treated mice. Taken together, these results suggest that this $CD8^+$ subset of T cells play a positive role in the host defense against SARS-CoV infection.

DISCUSSION

The data presented in this study greatly extend in at least seven ways our previous report concerning the differential pathogenesis of SARS-CoV infection in hACE2 Tg mouse lineages established in our laboratories (32). First, we demonstrated that among five lineages of hACE2 Tg mice, all of which exhibited clinical manifestations of various severity following SARS-CoV infection, mice three lineages (AC70, AC50, and AC12) inevitably died within a week after infection, whereas mice of the other two (AC63 and AC22) eventually recovered from the illness without suffering any mortality (Table 1). Such a strikingly different disease outcome elicited in these Tg mice in response to SARS-CoV infection provides an ample opportunity for studying the likely impact of the complex virus-host interactions on the pathogenesis of SARS-CoV in an animal model. Second, by using hACE2 Tg AC70 and AC22 mice as the lethal and nonlethal models of SARS-CoV infection, respectively, we established the kinetics of the disease course (i.e., illness score and weigh loss) and/or the rate of mortality (Fig. 2). These results clearly indicated that despite the similar onset and progression of clinical manifestations,

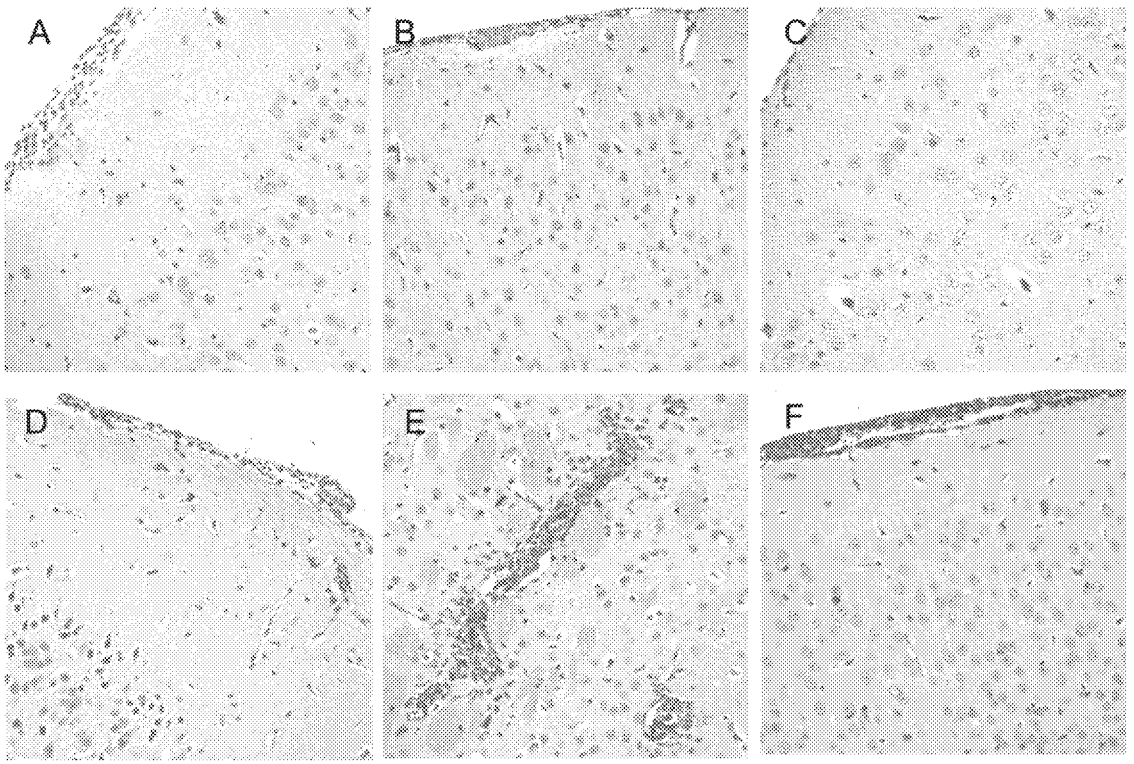

FIG. 7. Brain pathology of SARS-CoV-infected AC70 and AC22 mice. Brains harvested from infected mice daily from day 1 to 5 for both hACE2 lineages and every 3 to 4 days thereafter were paraffin embedded, sectioned, and stained with hematoxylin and eosin. No obvious brain pathology was observed prior to days 3 and 4 in infected AC70 and AC22 mice, respectively. Perivascular cuffing in the meninge was observed only in a single infected AC70 mouse at day 3 (A). Very little pathology, if any, could be detected in the brains of infected AC70 mice thereafter (B [day 4] and C [day 5]). In contrast, perivacular cuffing was consistently detected in all infected AC22 mice, starting at day 4 (D). A time-dependent and prominent inflammatory infiltration was observed at day 6 (E). Perivascular cuffing persisted through day 21 (F), when the study was terminated. Original magnifications, ×20.

infected AC22 mice exhibited much milder disease than did infected AC70 mice and completely recovered around day 17 p.i. Third, we showed the kinetics of replication and the cellular distribution of SARS-CoV within the lungs and brains, two of the most severely affected tissues, and identified bronchial epithelial cells, alveolar epithelial cells, and neuronal cells as the main target cells of SARS-CoV infection in both lineages (Fig. 3 to 5). Additionally, the significant delay in detecting brain infection in both lineages, compared to the early and intense viral replication within the lungs, clearly indicated that SARS-CoV infection was first established in the respiratory system before spreading to the CNS, an observation consistent with our previous finding and an earlier report by McCray and colleagues on hACE2 Tg mice (21, 32). However, after the same group presented a more thorough examination, they concluded that SARS-CoV enters the brains of K18-hACE2 Tg mice primarily via the olfactory bulb, resulting in extensive brain infection (22); whether this olfactory route of SARS-CoV entry could also be responsible for the subsequent intense brain infection in our Tg mice requires additional studies. Fourth, while the overall lung pathologies presented the two lineages were largely indistinguishable (Fig. 6), the pathological features within the brains were markedly different with regard to the cellular responses, in that infected AC22 but not AC70 mice consistently exhibited a time-dependent infiltration of inflammatory cells in the brains, as revealed by the prominent accumulation of mononuclear cells and activation of microglial cells within the CNS (Fig. 7). Fifth, despite the minimal cellular responses to SARS-CoV infection within the brains, AC70 mice were as capable as AC22 mice in producing elevated levels of proinflammatory cytokines and chemokines there in response to SARS-CoV infection (Fig. 9). However, AC22 mice appeared to be superior to AC70 mice in inducing inflammatory responses within the lungs, where there was a more intense secretion of an array of soluble inflammatory mediators, some of which were not detected in infected AC70 mice (Fig. 8). Sixth, our results clearly demonstrated that SARS-CoV infection in hACE2 Tg mice can cause a generalized suppression of host immunity, at least in part through the depletion of T cells (Tables 2 and 3; Fig. 10). Interestingly, the extent of T-cell loss, especially loss of the CD8 subset, appeared to positively correlate with the susceptibility of mice to the lethal SARS-CoV infection. Specifically, in contrast to the drastically reduced number of CD8 T cells in the lethality-sensitive AC70 mice, the number of this CD8 T-cell subset was basically not affected in the resistant AC22 mice. Finally, our study also identifies the positive role of CD8 T cells in protecting AC22 mice against excessive respiratory infection and pathology and the onset of illness (e.g., weight loss) (Fig. 11).

SARS has been generally recognized as an acute viral pneumonia, with the lungs as its main pathological target. However, we found that SARS-CoV, like other animal and human coro-

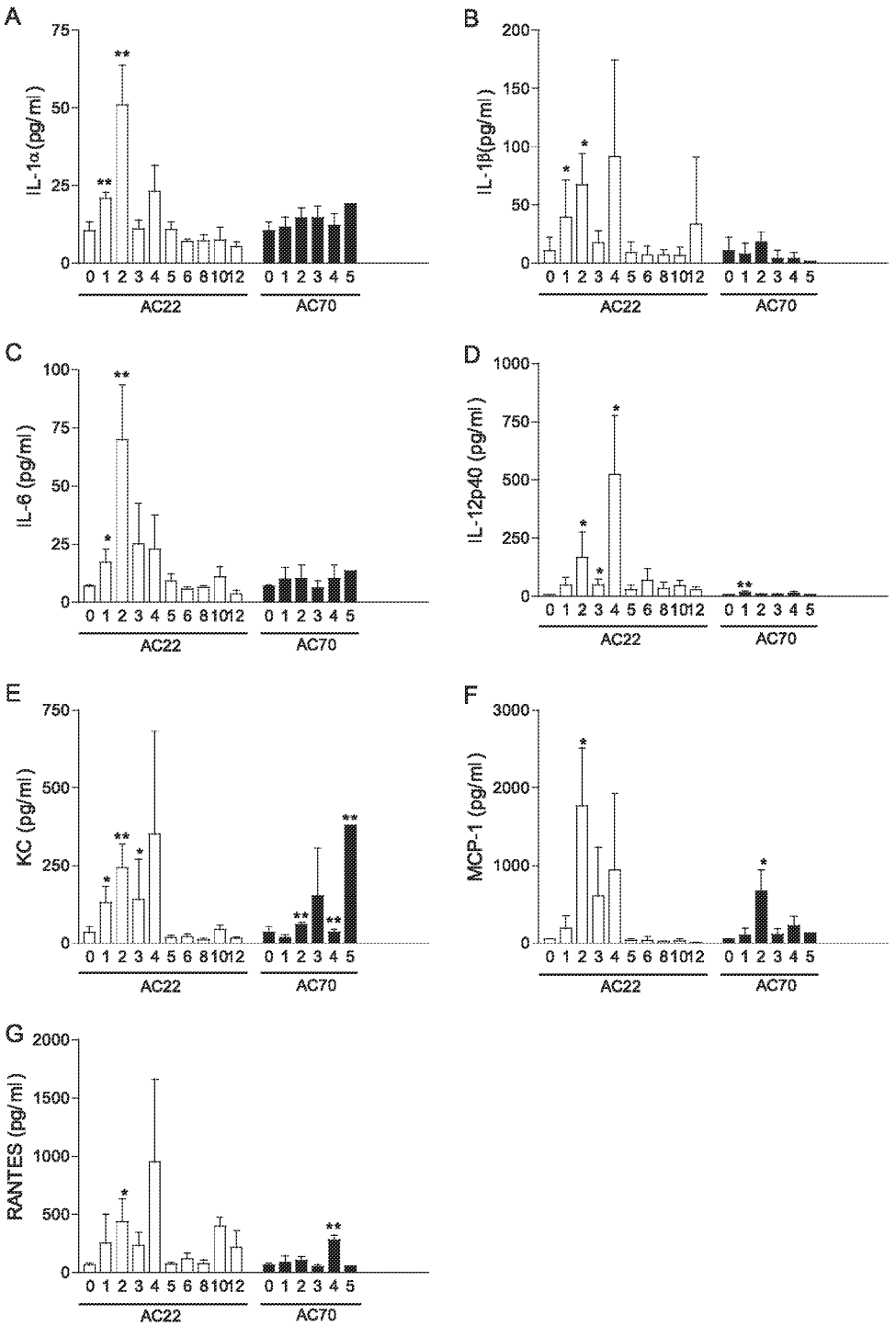

FIG. 8. Kinetics of the cytokine responses in the lungs of SARS-CoV-infected AC70 and AC22 mice. Lung homogenates derived from AC70 and AC22 mice at the indicated time points after infection were used to assess the levels of chemokines and cytokines by Bio-Plex analysis. Duplicate samples of individual specimens were assayed. Results are shown as means ± standard deviations for three animals at the indicated time points, except for day 5, at which only two AC70 mice that survived the infection were used. *, $P < 0.05$; **, $P < 0.01$ (Student's t test, compared to mock-infected mice).

naviruses, could infect the CNS in our Tg models. In fact, studies of brain sections obtained from SARS patients who died as a result of this disease have clearly demonstrated, by IHC, real-time PCR, in situ hybridization, and electron microscopy, the expression of SARS-CoV exclusively within the neuronal cells (5, 10, 40). The susceptibility of neuronal cells to SARS-CoV infection has been underscored by recent studies using both wild-type and hACE2 Tg mice infected with either

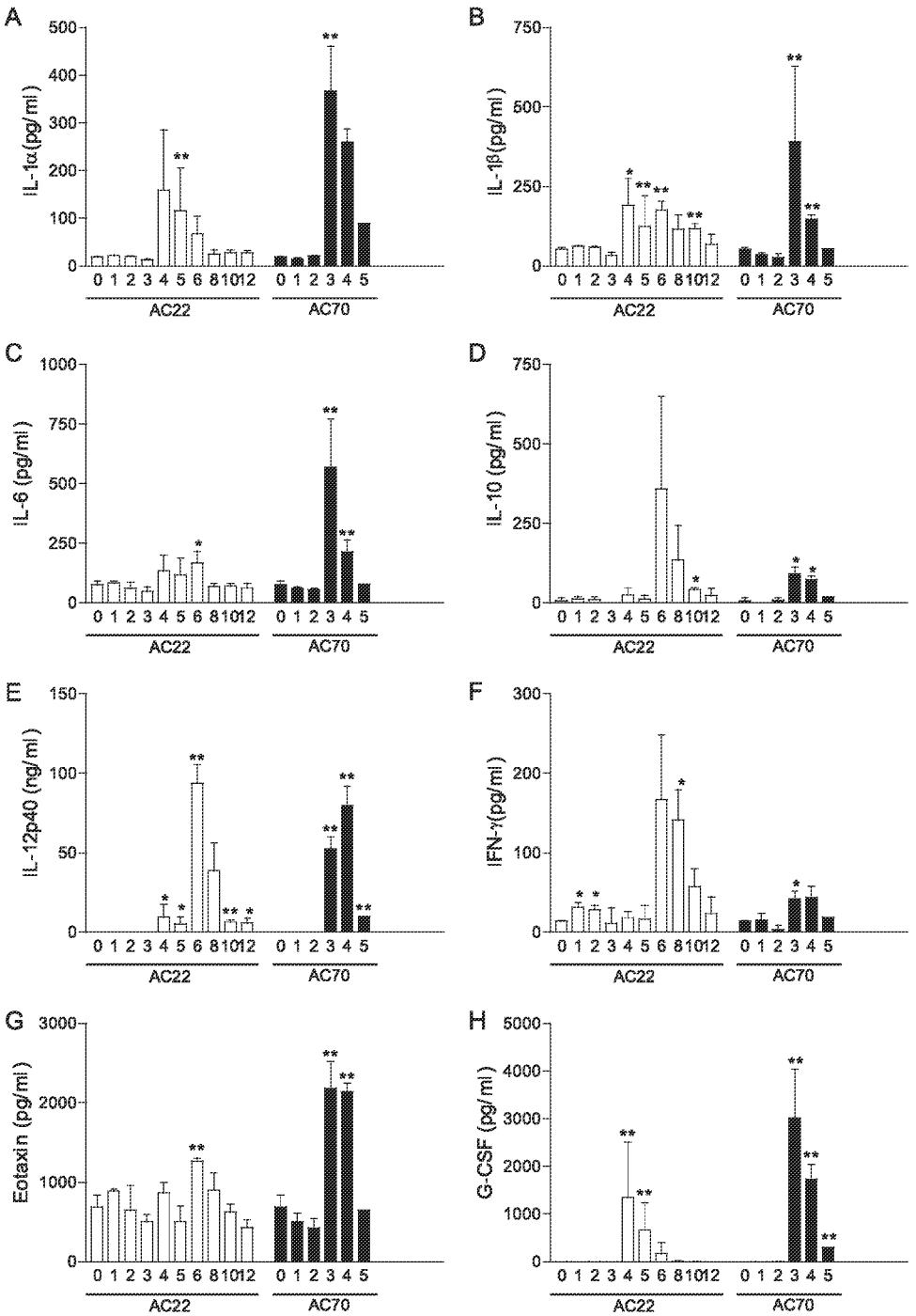

FIG. 9. Kinetics of the cytokine responses in the brains of SARS-CoV-infected AC70 and AC22 mice. Homogenates of the brains harvested from AC70 and AC22 mice at the indicated time points after SARS-CoV infection were used to measure the expression of various cytokines and chemokines by Bio-Plex analysis. Duplicate samples of individual specimens were assayed. Results are shown as means ± standard deviations for three animals at the indicated time points, except for day 5, at which only two AC70 mice that survived the infection were used. *, $P < 0.05$; **, $P < 0.01$ (Student's t test, compared to mock-infected mice).

the clinical isolates or mouse-adapted SARS-CoV (11, 26, 29, 35; C.-T. K. Tseng et al., unpublished data). In addition, two of the four human glioma cell lines tested in our laboratories appeared to be permissive to productive SARS-CoV infection (Tseng et al., unpublished data). Thus, identification of the neuronal cells as the major target of SARS-CoV infection in the brains of both lineages of Tg mice further confirmed their permissiveness to this CoV infection.

Early pathological studies with lung specimens obtained from the patients who died of SARS and in whom the disease progressed slowly identified type I and II alveolar pneumocytes and, possibly, pulmonary macrophages as the primary targets

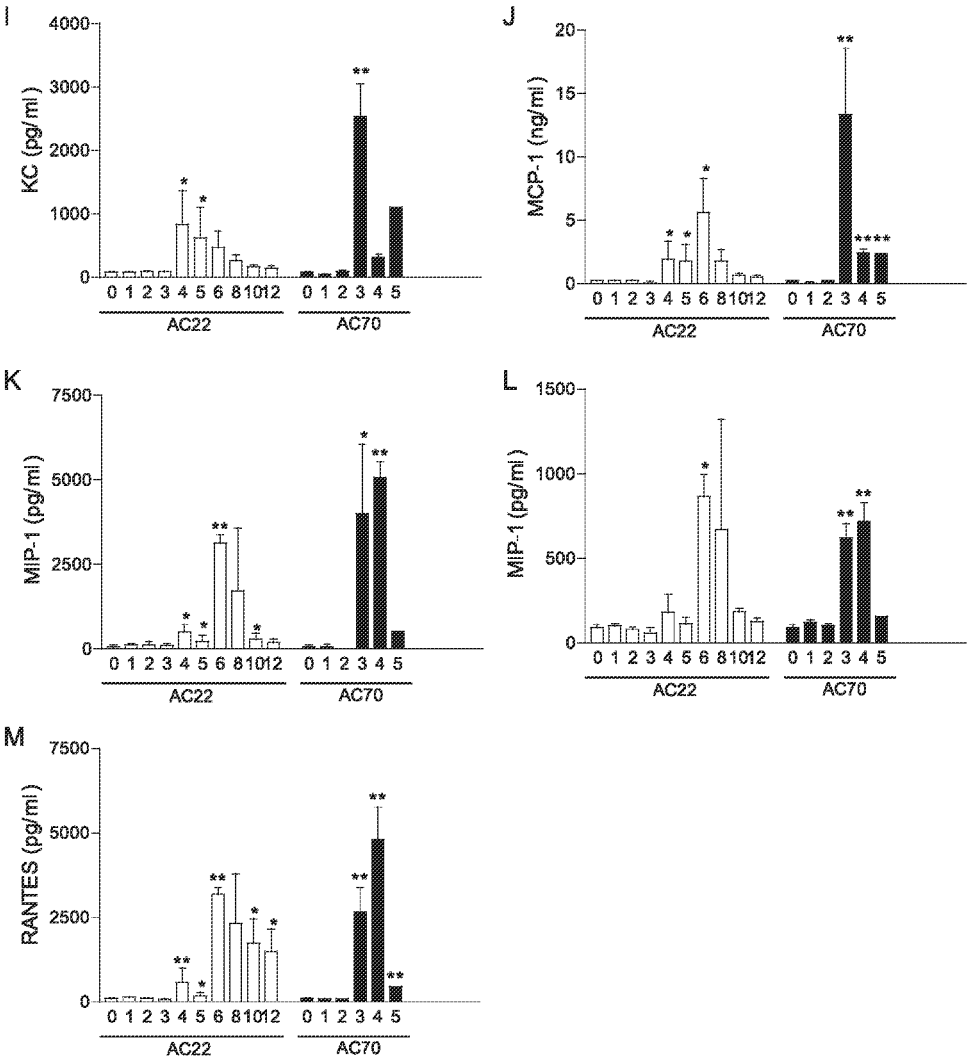

FIG. 9—*Continued.*

of SARS-CoV infection (2, 24, 31). However, the possibility that the pathogenesis might initiate within the respiratory bronchioles came about due to the revelation of prominent bronchitis with a marked necrosis of epithelial cells, loss of cilia, squamous metaplasia, and fibrin deposition within the bronchi in the lungs of patients who died following a more rapid clinical course of SARS (7, 24). Furthermore, human primary bronchial and other ciliated airway epithelial cells

TABLE 2. Total cell counts and lymphocyte subsets in the spleens of SARS-CoA-infected AC70 and AC22 mice and mock-infected control mice

Cells	AC22 mice					AC70 mice				
	No. of cells (10^6) or ratio[a]				P[b]	No. of cells (10^6) or ratio				P
	Mock infection		SARS infection			Mock infection		SARS infection		
	Mean	SD	Mean	SD		Mean	SD	Mean	SD	
Splenocytes	130.0	10.0	130.0	10.0	0.698	166.7	11.5	100.0	28.3	0.032
CD4 cells	41.4	2.5	25.4	2.7	0.005	52.3	3.9	32.1	7.5	0.025
CD8 cells	19.9	0.7	18.1	4.2	0.652	31.0	1.9	7.0	0.1	0.001
CD4/CD8 ratio	2.1	0.0	1.4	0.3	0.095	1.7	0.2	4.6	1.2	0.018
B cells	49.4	2.9	58.7	9.4	0.278	58.1	1.0	43.5	9.6	0.060
Non-T non-B cells	24.3	1.0	27.9	7.5	0.599	25.2	8.7	17.4	11.4	0.414

[a] Means and standard deviations are for three or four mice.
[b] Student's *t* test for mock-infected versus infected mice.

TABLE 3. ConA-stimulated proliferation of splenic T cells in uninfected and SARS-CoV-infected AC70 and AC22 mice

Mice	Mock infection						SARS-CoV infection					
	[^{3}H]thymidine uptake (cpm)				SI[a]		[^{3}H]thymidine uptake (cpm)				SI	
	Stimulated cultures		Unstimulated cultures				Stimulated cultures		Unstimulated cultures			
	Mean	SD	Mean	SD	Mean	SD	Mean	SD	Mean	SD	Mean	SD
AC70	4,370	1,790	86	39	54	27	552	246	138	138	6.0	3
AC22	4,700	725	68	14	70	15	1,845	841	83	19	24	13

[a] SI, stimulation index (cpm of ConA-stimulated cultures/cpm of unstimulated cultures).

have also been demonstrated, in vitro, to be permissive to productive SARS-CoV infection (14, 27, 34). Thus, our IHC study results, which revealed epithelial cells lining the respiratory tract, especially the bronchi and bronchioles, and alveolar epithelial cells as the prime cells harboring SARS-CoV, led us to suggest that SARS-CoV infection in hACE2 Tg mice may induce a faster course of clinical illness, perhaps similar to that in SARS patients having a rapidly progressing form of the disease.

SARS has been proposed to stem from exuberant innate inflammatory responses with diffuse alveolar damages as the most characteristic pathological feature (6, 7, 24). Specifically, SARS-CoV infection has been reported to minimally induce the expression of antiviral cytokines (e.g., interferons and IL-12p40), moderately upregulate the expression of proinflammatory cytokines (e.g., tumor necrosis factor alpha and IL-6), and significantly promote the production of proinflammatory chemokines (e.g., MIP-1a, IP-10, RANTES, and MCP-1) in patients (17, 28). Elevated and prolonged expressions of chemokines (i.e., MIP-1, IP-10, CXCL8, and CXCL9) have been

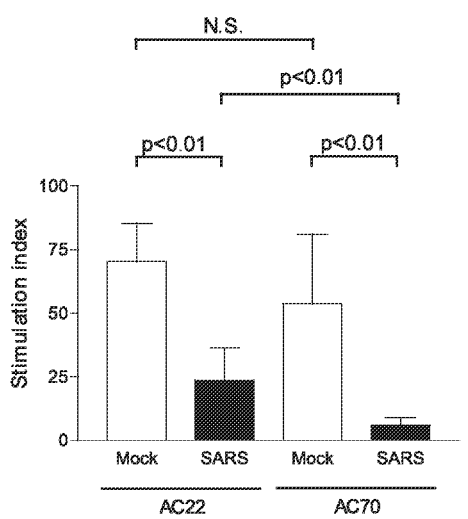

FIG. 10. SARS-CoV significantly inhibits ConA-mediated proliferation of T cells in infected AC70 and AC22 mice. AC70 and AC22 mice were either uninfected or infected (i.n.) with 10^6 $TCID_{50}$ SARS-CoV. Splenocytes were prepared from individual mice and tested for their proliferation in response to ConA (2.5 μg/ml) stimulation, as described in Materials and Methods. Student's *t* test was used to determine the *P* values between the indicated groups for statistical significance. N.S., not significant. Error bars indicate standard deviations.

detected not only in SARS patients but also in experimentally infected wild-type and lethality-sensitive hACE2 Tg mice (8, 10, 13, 32, 35, 36, 38). In this study, we extended this observation to hACE2 Tg mice that were resistant to the lethal SARS-CoV infection. Interestingly, while the kinetics and magnitude of the cytokine responses within each lineage appeared to positively correlate with the extent of viral replication in each tissue, no such correlation in the brain could be observed when findings for these two Tg lineages were compared.

The cellular sources and the overall impact of these virally induced inflammatory mediators (Fig. 8 and 9) on the pathogenesis and/or clearance of SARS-CoV remain to be determined. Neuronal cells have recently been shown to release abundant IL-6 in SARS-CoV-infected K18-hACE2 mice that rapidly succumbed to infection with minimal cellular infiltration within the brain (22). Thus, the overwhelming viral infection in the absence of readily detectable cellular infiltrates within the brains of infected AC70 mice makes neuronal cells and, possibly, other brain cells the likely producers of these inflammatory mediators within the brain. Despite the less profound brain infection, SARS-CoV-infected AC22 mice consistently showed a time-dependent infiltration of inflammatory cells. Thus, it is likely that infiltrating cells might effectively make up the shortfall of cytokine responses elicited by moderately infected brain cells in this Tg lineage. The ability to elicit an optimal acute inflammatory response is essential, not only to limit early microbial infections but also to ensure the onset of adaptive responses to effectively resolve the infections. However, an excess inflammatory response often leads to immune-mediated pathology and diseases. Thus, it is tempting to hypothesize that the highly elevated levels of inflammatory mediators detected in our study might contribute to exacerbated clinical and pathological outcomes of SARS-CoV-infected Tg mice. While it is highly desirable to determine which cytokine(s), alone or in combination, is likely to be responsible for the onset of clinical illness and even death in infected Tg mice, choosing which cytokine(s) from minimums of 7 and 13 potential candidates within the lungs and brain, respectively, is a major undertaking and is beyond the scope of this study.

It has been shown that SARS-CoV infection in clinical patients was accompanied by a transient, but extensive, lymphopenia with a preferential reduction in the number of CD4 and CD8 T cells (4, 12, 18, 39). Importantly, the severity of T-cell loss has been positively correlated with an adverse outcome in SARS patients. Thus, a much more pronounced T-cell loss in the lethality-susceptible AC70 mice than in the lethality-resistant AC22 mice extends this correlation to the mouse

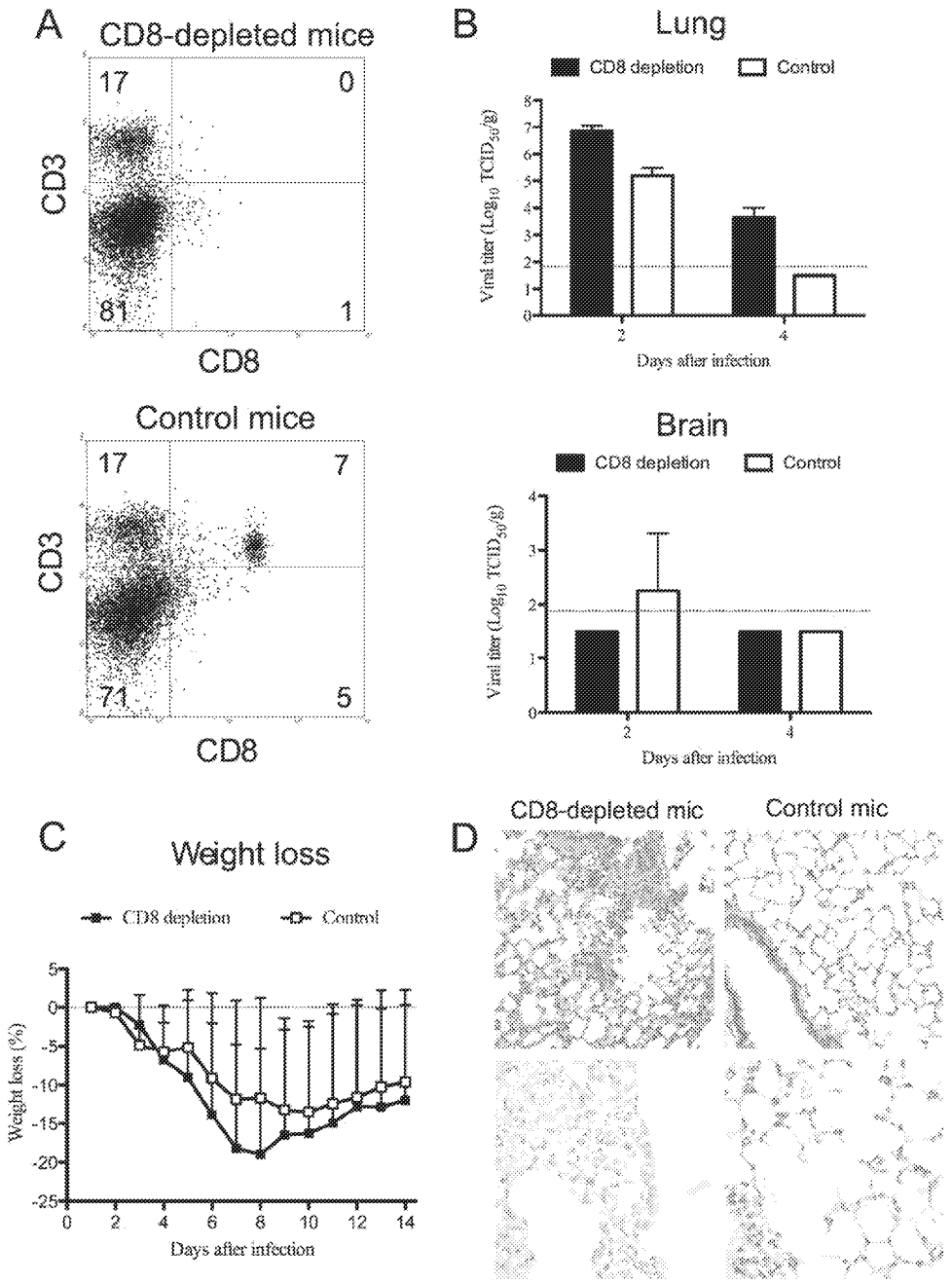

FIG. 11. Exacerbated pathogenesis of SARS-CoV infection in CD8-depleted Tg AC22 mice. Two groups of Tg AC22 mice (12 mice per group) were subjected to multiple doses (i.p.) of rat anti-mouse CD8 monoclonal antibody and an isotype-matched irrelevant rat monoclonal antibody (as control), respectively, as described in Materials and Methods. They were then infected i.n. with 10^6 $TCID_{50}$ SARS-CoV. Two mice/group were sacrificed after two doses of antibody treatment for assessing by flow cytometry the efficacy of antibody-mediated CD8 depletion in the spleens, whereas the effect of CD8 depletion on the pathogenesis of SARS-CoV infection was evaluated by virologic, clinical, and pathological parameters, as described in the text. Briefly, two additional mice were sacrificed at days 2 and 4 p.i. to allow assessment of virus infectivity and pathology in the lungs and brains, and the remaining mice were monitored for the onset of illness (i.e., weight loss). It appeared that a two-dose specific-antibody treatment regimen effectively depleted most of the $CD8^+$ T cells from the spleens (A). SARS-CoV infection of CD8-depleted mice resulted in increased infection in the lungs, but not in the brains, at both days 2 and 4 p.i. (B). This was accompanied by an increased weight loss (C), as well as more pronounced histopathology and the retention of viral NC antigen at day 4 p.i., as revealed by hematoxylin and eosin staining and IHC, respectively (D).

model for SARS-CoV infection. Although the underlying mechanism of SARS-CoV-associated lymphopenia in patients, as well as in the Tg mice described in this study, remains unclear, the absence of ACE2 expression in lymphocytes (11) makes the direct lysis of lymphocytes by this virus unlikely. Sequestration of lymphocytes in affected tissues also seems unlikely, at least in our AC70 mice, in which SARS-CoV infection failed to elicit a persistent infiltration of mononuclear

cells within the brain. Rather, cytokine-mediated apoptosis of uninfected lymphocytes may be the cause of acute lymphopenia, as suggested by others (12, 37). In this regard, further investigation is needed to discern whether some of the cytokines that were produced by SARS-CoV-infected Tg mice could cause apoptosis of T cells.

While a profound T-cell loss was readily detectable in our Tg mouse lineages, especially the lethality-susceptible AC70 mice, neither B cells nor non-T non-B lymphocytes were noticeably affected (Table 2), which led to the possibility that T cells were the preferred targets for manipulation by SARS-CoV in our Tg mouse model. More strikingly, in contrast to the grossly diminished number of CD8 T cells in AC70 mice which rapidly succumbed to lethal infection, this T-cell subset was largely unaffected by SARS-CoV in the lethality-resistant AC22 mice, a finding which implied that this CD8 subset of T cells might have a protective role in AC22 mice against SARS-CoV infection. We employed a depletion technique using rat anti-mouse CD8 antibody to investigate the role that $CD8^+$ T cells might have.

Elimination of most of the CD8 T cells in the spleens of AC22 mice resulted in an increased respiratory infection, accompanied by more intense lung pathology, compared to that in control mice (Fig. 11B and D). Although $CD8^+$ T cells were also effective in attenuating weight loss (Fig. 11C), we noted that the extent of weigh loss in infected AC22 mice treated with control rat IgG antibody was much less than that in untreated mice (10 to 15% versus 35% weight loss). High-dose intravenous IgG has been widely used as a potent immune modulator for the treatment of autoimmune diseases and many infectious diseases. This modulation occurs most likely, in part, through the Fc portion of the IgG molecule (25). Thus, multiple i.p. injections with 50 μg/injection of irrelevant rat IgG into AC22 mice might provide a yet-to-be identified immune regulatory mechanism in protecting against excess infection and weight loss. While $CD8^+$ T cells have a protective role against SARS-CoV infection, the exact mechanisms underlying this CD8-mediated protection in AC22 mice remain undefined. Because the clearance of many viral infections requires antigen-specific T cells, it is tempting to hypothesize that these protective $CD8^+$ T cells were likely SARS-CoV specific. The development of primary T-cell responses in an immunocompetent host usually takes about 4 days after an initial encounter with invading pathogens. Thus, the observation that a noticeable difference in the virally induced weight loss between CD8-depleted and control AC22 mice could not be detected until day 5 and continued through day 8 p.i. (Fig. 11C) might argue for the SARS-CoV-specific nature of these protective $CD8^+$ T cells. While $CD8^+$ T cells could attenuate the pathogenesis of SARS-CoV, other cellular elements of the immune system, especially CD4 T cells, are likely needed to provide more complete protection against SARS-CoV in our Tg mouse model. Additional studies are warranted to identify epitope-specific $CD8^+$ T cells and determine the contribution of $CD4^+$ T cells in the host defense against SARS-CoV in our Tg mouse model.

In summary, our studies have provided cellular and molecular insights into the differential regulation of host immune responses against SARS-CoV infection in two lineages of hACE2 Tg mice that were either susceptible or resistant to lethal SARS-CoV infection. Importantly, the less severe loss of T cells, accompanied by the ability to recover from SARS-CoV-associated acute clinical illness, makes our lethality-resistant lineage, i.e., AC22, particularly useful for dissecting both the innate and adaptive arms of the host immunity against the SARS-CoV infection. In addition, the fatal outcome of the disease in AC70 mice make this lineage attractive as a stringent model for adoptive transfer studies aimed at evaluation of the molecular and cellular bases responsible for the protection against SARS-CoV infection.

ACKNOWLEDGMENTS

We thank Mardelle Susman for her help in preparing the manuscript. We also thank Patrick Newman, Junhui Jia, Jignesh Patel, and Tonia Garron for their excellent technical support.

This work was supported by National Institutes of Health grants R21AI072201 (to C.K.T.) and R21AI063118 (to T.S.C.), a Career Development Grant award (to C.K.T.) through the Western Regional Center of Excellence for Biodefense and Emerging Infectious Diseases (U54 AI057156), and subcontract awards on SARS from the Viral Respiratory Pathogens Research Unit (NO1 AI30039) (to C.K.T.) and U.S. Based Collaboration in Emerging Viral and Prior Diseases (NO1 AI25489) (to C.J.P.). T.Y. was supported by the James W. McLaughlin Fellowship Fund.

REFERENCES

1. **Cheung, C. Y., L. L. Poon, A. S. Lau, W. Luk, Y. L. Lau, K. F. Shortridge, S. Gordon, Y. Guan, and J. S. Peiris.** 2002. Induction of proinflammatory cytokines in human macrophages by influenza A (H5N1) viruses: a mechanism for the unusual severity of human disease? Lancet **360:**1831–1837.
2. **Chow, K. C., C. H. Hsiao, T. Y. Lin, C. L. Chen, and S. H. Chiou.** 2004. Detection of severe acute respiratory syndrome-associated coronavirus in pneumocytes of the lung. Am. J. Clin. Pathol. **121:**574–580.
3. **Claas, E. C., A. D. Osterhaus, R. van Beek, J. C. De Jong, G. F. Rimmelzwaan, D. A. Senne, S. Krauss, K. F. Shortridge, and R. G. Webster.** 1998. Human influenza A H5N1 virus related to a highly pathogenic avian influenza virus. Lancet **351:**472–477.
4. **Cui, W., Y. Fan, W. Wu, F. Zhang, J. Y. Wang, and A. P. Ni.** 2003. Expression of lymphocytes and lymphocyte subsets in patients with severe acute respiratory syndrome. Clin. Infect. Dis. **37:**857–859.
5. **Ding, Y., L. He, Q. Zhang, Z. Huang, X. Che, J. Hou, H. Wang, H. Shen, L. Qiu, Z. Li, J. Geng, J. Cai, H. Han, X. Li, W. Kang, D. Weng, P. Liang, and S. Jiang.** 2004. Organ distribution of severe acute respiratory syndrome (SARS) associated coronavirus (SARS-CoV) in SARS patients: implications for pathogenesis and virus transmission pathways. J. Pathol. **203:**622–630.
6. **Ding, Y., H. Wang, H. Shen, Z. Li, J. Geng, H. Han, J. Cai, X. Li, W. Kang, D. Weng, Y. Lu, D. Wu, L. He, and K. Yao.** 2003. The clinical pathology of severe acute respiratory syndrome (SARS): a report from China. J. Pathol. **200:**282–289.
7. **Franks, T. J., P. Y. Chong, P. Chui, J. R. Galvin, R. M. Lourens, A. H. Reid, E. Selbs, C. P. McEvoy, C. D. Hayden, J. Fukuoka, J. K. Taubenberger, and W. D. Travis.** 2003. Lung pathology of severe acute respiratory syndrome (SARS): a study of 8 autopsy cases from Singapore. Hum. Pathol. **34:**743–748.
8. **Glass, W. G., K. Subbarao, B. Murphy, and P. M. Murphy.** 2004. Mechanisms of host defense following severe acute respiratory syndrome-coronavirus (SARS-CoV) pulmonary infection of mice. J. Immunol. **173:**4030–4039.
9. **Graham, B. S., L. A. Bunton, P. F. Wright, and D. T. Karzon.** 1991. Role of T lymphocyte subsets in the pathogenesis of primary infection and rechallenge with respiratory syncytial virus in mice. J. Clin. Investig. **88:**1026–1033.
10. **Gu, J., E. Gong, B. Zhang, J. Zheng, Z. Gao, Y. Zhong, W. Zou, J. Zhan, S. Wang, Z. Xie, H. Zhuang, B. Wu, H. Zhong, H. Shao, W. Fang, D. Gao, F. Pei, X. Li, Z. He, D. Xu, X. Shi, V. M. Anderson, and A. S. Leong.** 2005. Multiple organ infection and the pathogenesis of SARS. J. Exp. Med. **202:**415–424.
11. **Hamming, I., W. Timens, M. L. Bulthuis, A. T. Lely, G. J. Navis, and H. van Goor.** 2004. Tissue distribution of ACE2 protein, the functional receptor for SARS coronavirus. A first step in understanding SARS pathogenesis. J. Pathol. **203:**631–637.
12. **He, Z., C. Zhao, Q. Dong, H. Zhuang, S. Song, G. Peng, and D. E. Dwyer.** 2005. Effects of severe acute respiratory syndrome (SARS) coronavirus infection on peripheral blood lymphocytes and their subsets. Int. J. Infect. Dis. **9:**323–330.
13. **Huang, K. J., I. J. Su, M. Theron, Y. C. Wu, S. K. Lai, C. C. Liu, and H. Y. Lei.** 2005. An interferon-gamma-related cytokine storm in SARS patients. J. Med. Virol. **75:**185–194.

14. **Jia, H. P., D. C. Look, L. Shi, M. Hickey, L. Pewe, J. Netland, M. Farzan, C. Wohlford-Lenane, S. Perlman, and P. B. McCray, Jr.** 2005. ACE2 receptor expression and severe acute respiratory syndrome coronavirus infection depend on differentiation of human airway epithelia. J. Virol. **79:**14614–14621.
15. **Ksiazek, T. G., D. Erdman, C. S. Goldsmith, S. R. Zaki, T. Peret, S. Emery, S. Tong, C. Urbani, J. A. Comer, W. Lim, P. E. Rollin, S. F. Dowell, A. E. Ling, C. D. Humphrey, W. J. Shieh, J. Guarner, C. D. Paddock, P. Rota, B. Fields, J. DeRisi, J. Y. Yang, N. Cox, J. M. Hughes, J. W. LeDuc, W. J. Bellini, and L. J. Anderson.** 2003. A novel coronavirus associated with severe acute respiratory syndrome. N. Engl. J. Med. **348:**1953–1966.
16. **Lau, S. K., P. C. Woo, K. S. Li, Y. Huang, H. W. Tsoi, B. H. Wong, S. S. Wong, S. Y. Leung, K. H. Chan, and K. Y. Yuen.** 2005. Severe acute respiratory syndrome coronavirus-like virus in Chinese horseshoe bats. Proc. Natl. Acad. Sci. USA **102:**14040–14045.
17. **Law, H. K., C. Y. Cheung, H. Y. Ng, S. F. Sia, Y. O. Chan, W. Luk, J. M. Nicholls, J. S. Peiris, and Y. L. Lau.** 2005. Chemokine up-regulation in SARS-coronavirus-infected, monocyte-derived human dendritic cells. Blood **106:**2366–2374.
18. **Li, T., Z. Qiu, L. Zhang, Y. Han, W. He, Z. Liu, X. Ma, H. Fan, W. Lu, J. Xie, H. Wang, G. Deng, and A. Wang.** 2004. Significant changes of peripheral T lymphocyte subsets in patients with severe acute respiratory syndrome. J. Infect. Dis. **189:**648–651.
19. **Li, W., M. J. Moore, N. Vasilieva, J. Sui, S. K. Wong, M. A. Berne, M. Somasundaran, J. L. Sullivan, K. Luzuriaga, T. C. Greenough, H. Choe, and M. Farzan.** 2003. Angiotensin-converting enzyme 2 is a functional receptor for the SARS coronavirus. Nature **426:**450–454.
20. **Li, W., Z. Shi, M. Yu, W. Ren, C. Smith, J. H. Epstein, H. Wang, G. Crameri, Z. Hu, H. Zhang, J. Zhang, J. McEachern, H. Field, P. Daszak, B. T. Eaton, S. Zhang, and L. F. Wang.** 2005. Bats are natural reservoirs of SARS-like coronaviruses. Science **310:**676–679.
21. **McCray, P. B., Jr., L. Pewe, C. Wohlford-Lenane, M. Hickey, L. Manzel, L. Shi, J. Netland, H. P. Jia, C. Halabi, C. D. Sigmund, D. K. Meyerholz, P. Kirby, D. C. Look, and S. Perlman.** 2007. Lethal infection of K18-hACE2 mice infected with severe acute respiratory syndrome coronavirus. J. Virol. **81:**813–821.
22. **Netland, J., D. K. Meyerholz, S. Moore, M. Cassell, and S. Perlman.** 2008. Severe acute respiratory syndrome coronavirus infection causes neuronal death in the absence of encephalitis in mice transgenic for human ACE2. J. Virol. **82:**7264–7275.
23. **Nicholls, J. M., J. Butany, L. L. Poon, K. H. Chan, S. L. Beh, S. Poutanen, J. S. Peiris, and M. Wong.** 2006. Time course and cellular localization of SARS-CoV nucleoprotein and RNA in lungs from fatal cases of SARS. PLoS Med. **3:**e27.
24. **Nicholls, J. M., L. L. Poon, K. C. Lee, W. F. Ng, S. T. Lai, C. Y. Leung, C. M. Chu, P. K. Hui, K. L. Mak, W. Lim, K. W. Yan, K. H. Chan, N. C. Tsang, Y. Guan, K. Y. Yuen, and J. S. Peiris.** 2003. Lung pathology of fatal severe acute respiratory syndrome. Lancet **361:**1773–1778.
25. **Nimmerjahn, F., and J. V. Ravetch.** 2007. The antiinflammatory activity of IgG: the intravenous IgG paradox. J. Exp. Med. **204:**11–15.
26. **Roberts, A., and K. Subbarao.** 2006. Animal models for SARS. Adv. Exp. Med. Biol. **581:**463–471.
27. **Sims, A. C., S. E. Burkett, B. Yount, and R. J. Pickles.** 2008. SARS-CoV replication and pathogenesis in an in vitro model of the human conducting airway epithelium. Virus Res. **133:**33–44.
28. **Spiegel, M., A. Pichlmair, L. Martinez-Sobrido, J. Cros, A. Garcia-Sastre, O. Haller, and F. Weber.** 2005. Inhibition of beta interferon induction by severe acute respiratory syndrome coronavirus suggests a two-step model for activation of interferon regulatory factor 3. J. Virol. **79:**2079–2086.
29. **Subbarao, K., and A. Roberts.** 2006. Is there an ideal animal model for SARS? Trends Microbiol. **14:**299–303.
30. **To, K. F., P. K. Chan, K. F. Chan, W. K. Lee, W. Y. Lam, K. F. Wong, N. L. Tang, D. N. Tsang, R. Y. Sung, T. A. Buckley, J. S. Tam, and A. F. Cheng.** 2001. Pathology of fatal human infection associated with avian influenza A H5N1 virus. J. Med. Virol. **63:**242–246.
31. **To, K. F., and A. W. Lo.** 2004. Exploring the pathogenesis of severe acute respiratory syndrome (SARS): the tissue distribution of the coronavirus (SARS-CoV) and its putative receptor, angiotensin-converting enzyme 2 (ACE2). J. Pathol. **203:**740–743.
32. **Tseng, C. T., C. Huang, P. Newman, N. Wang, K. Narayanan, D. M. Watts, S. Makino, M. M. Packard, S. R. Zaki, T. S. Chan, and C. J. Peters.** 2007. Severe acute respiratory syndrome coronavirus infection of mice transgenic for the human angiotensin-converting enzyme 2 virus receptor. J. Virol. **81:**1162–1173.
33. **Tseng, C. T., L. A. Perrone, H. Zhu, S. Makino, and C. J. Peters.** 2005. Severe acute respiratory syndrome and the innate immune responses: modulation of effector cell function without productive infection. J. Immunol. **174:**7977–7985.
34. **Tseng, C. T., J. Tseng, L. Perrone, M. Worthy, V. Popov, and C. J. Peters.** 2005. Apical entry and release of severe acute respiratory syndrome-associated coronavirus in polarized Calu-3 lung epithelial cells. J. Virol. **79:**9470–9479.
35. **Tsui, P. T., M. L. Kwok, H. Yuen, and S. T. Lai.** 2003. Severe acute respiratory syndrome: clinical outcome and prognostic correlates. Emerg. Infect. Dis. **9:**1064–1069.
36. **Ward, S. E., M. R. Loutfy, L. M. Blatt, K. A. Siminovitch, J. Chen, A. Hinek, B. Wolff, D. H. Pham, H. Deif, E. A. LaMere, K. C. Kain, G. A. Farcas, P. Ferguson, M. Latchford, G. Levy, L. Fung, J. W. Dennis, E. K. Lai, and E. N. Fish.** 2005. Dynamic changes in clinical features and cytokine/chemokine responses in SARS patients treated with interferon alfacon-1 plus corticosteroids. Antivir. Ther. **10:**263–275.
37. **Weiss, S. R., and S. Navas-Martin.** 2005. Coronavirus pathogenesis and the emerging pathogen severe acute respiratory syndrome coronavirus. Microbiol. Mol. Biol. Rev. **69:**635–664.
38. **Wong, C. K., C. W. Lam, A. K. Wu, W. K. Ip, N. L. Lee, I. H. Chan, L. C. Lit, D. S. Hui, M. H. Chan, S. S. Chung, and J. J. Sung.** 2004. Plasma inflammatory cytokines and chemokines in severe acute respiratory syndrome. Clin. Exp. Immunol. **136:**95–103.
39. **Wong, R. S., A. Wu, K. F. To, N. Lee, C. W. Lam, C. K. Wong, P. K. Chan, M. H. Ng, L. M. Yu, D. S. Hui, J. S. Tam, G. Cheng, and J. J. Sung.** 2003. Haematological manifestations in patients with severe acute respiratory syndrome: retrospective analysis. BMJ **326:**1358–1362.
40. **Xu, J., S. Zhong, J. Liu, L. Li, Y. Li, X. Wu, Z. Li, P. Deng, J. Zhang, N. Zhong, Y. Ding, and Y. Jiang.** 2005. Detection of severe acute respiratory syndrome coronavirus in the brain: potential role of the chemokine mig in pathogenesis. Clin. Infect. Dis. **41:**1089–1096.